Published in final edited form as:

Nat Phys. 2020 ; 16(1): . doi:10.1038/s41567-019-0673-7.

Microwave-to-optics conversion using a mechanical oscillator in its quantum groundstate

Moritz Forsch[1,*], **Robert Stockill**[1,*], **Andreas Wallucks**[1], **Igor Marinković**[1], **Claus Gärtner**[1,2], **Richard A. Norte**[1,3], **Frank van Otten**[4], **Andrea Fiore**[4], **Kartik Srinivasan**[5], **Simon Gröblacher**[1,†]

[1]Kavli Institute of Nanoscience, Department of Quantum Nanoscience, Delft University of Technology, 2628CJ Delft, The Netherlands

[2]Vienna Center for Quantum Science and Technology (VCQ), Faculty of Physics, University of Vienna, A-1090 Vienna, Austria

[3]Department of Precision and Microsystems Engineering, Delft University of Technology, Mekelweg 2, 2628CD Delft, The Netherlands

[4]Department of Applied Physics and Institute for Photonic Integration, Eindhoven University of Technology, P.O. Box 513, 5600MB Eindhoven, The Netherlands

[5]Center for Nanoscale Science and Technology, National Institute of Standards and Technology, Gaithersburg, MD 20899, USA

Abstract

Conversion between signals in the microwave and optical domains is of great interest both for classical telecommunication, as well as for connecting future superconducting quantum computers into a global quantum network. For quantum applications, the conversion has to be both efficient, as well as operate in a regime of minimal added classical noise. While efficient conversion has been demonstrated using mechanical transducers, they have so far all operated with a substantial thermal noise background. Here, we overcome this limitation and demonstrate coherent conversion between GHz microwave signals and the optical telecom band with a thermal background of less than one phonon. We use an integrated, on-chip electro-opto-mechanical device that couples surface acoustic waves driven by a resonant microwave signal to an optomechanical crystal featuring a 2.7 GHz mechanical mode. We initialize the mechanical mode in its quantum groundstate, which allows us to perform the transduction process with minimal added thermal noise, while maintaining an optomechanical cooperativity >1, so that microwave photons mapped into the mechanical resonator are effectively upconverted to the optical domain. We further verify the preservation of the coherence of the microwave signal throughout the transduction process.

Research into novel quantum technologies is receiving significant attention for its potential to fundamentally transform how we receive, process and transmit information. In particular, major endeavors into building quantum processors and quantum simulators are currently

† s.groeblacher@tudelft.nl .

*These authors contributed equally to this work.

underway. Many leading efforts, including superconducting qubits [1] and quantum dots [2] share quantum information through photons in the microwave regime. While this allows for an impressive degree of quantum control [3], it also limits the distance the information can realistically travel before being lost [4]. At the same time, the field of optical quantum communication has already seen demonstrations over distance scales capable of providing real-world applications [5]. In particular, by transmitting information in the optical telecom band, fiber-based quantum networks over tens or even hundreds of kilometers can be envisaged [6]. In order to connect several quantum computing nodes over large distances into a quantum internet [7], it is therefore vital to be able to convert quantum information from the microwave to the optical domain, and back.

Several promising approaches have been taken to realize such a microwave to optics converter, most notably by trying to either directly couple the fields inside a non-linear crystal [8–11], by using rare earth ion doped crystals [12], magnons [13] or mechanical systems as a transducer [14–20]. Recent milestones include bi-directional operation [21], coherent coupling [22], as well as efficient conversion [23], all of which make use of a mechanical oscillator as the transducer. While high conversion efficiency has been a particular success with some mechanically-mediated frequency converters, the demonstration of intrinsic noise sources compatible with conversion of a quantum state has remained an outstanding challenge. For quantum information protocols, particularly those that can tolerate optical loss, the requirement of subphoton added noise necessitates that the converter contains less than one thermal excitation [24]. To this end, several experiments have recently demonstrated cooling of mechanical oscillators into the quantum groundstate of motion [25–27]. The low thermal occupation forms the basis for quantum control over mechanical states, with demonstrations including quantum state preparation [28–30] and entanglement between multiple mechanical degrees of freedom [31–33]. Reaching this occupation regime is complicated by the absorption of optical photons, while at the same time realizing sufficiently strong optomechanical cooperativity to suppress additional noise sources [34]. To date there has been no demonstration of a system with mechanically-mediated interfaces in both microwave and optical domains that operates in the quantum ground state.

In this work, we demonstrate microwave-to-optics conversion with an electro-opto-mechanical device, which contributes less than one quantum of thermal noise. We cryogenically cool a GHz frequency piezoelectric optomechanical crystal device into its quantum groundstate of motion and excite the mechanical mode using a microwave circuit through surface acoustic waves. Crucially, our system remains in the ground state while a drive of sufficient strength for upconversion from the mechanical to the optical domain is applied. This allows for conversion of a microwave pulse to the optical telecom band in a regime where we excite on average one phonon. As our converter features a noise source containing less than one photon, optimizing the electromechanical cooperativity [28, 35], the main efficiency bottleneck in our platform, will allow for the faithful transduction of a single photon from the microwave to optical domain.

Our microwave to optics converter consists of a one-dimensional optomechanical crystal (OMC) [36], which is mechanically coupled to an interdigital transducer (IDT) through

surface acoustic waves (see Fig. 1A). We fabricate the devices from a 250-nm thick GaAs layer, on a 3-μm $Al_{0.7}Ga_{0.3}As$ sacrificial layer, both epitaxially grown on a GaAs substrate. This material combines a large refractive index (n_{GaAs} = 3.37 at λ = 1550 nm) [37] and a non-zero piezoelectric coefficient (ϵ_{14} =−0.16 Cm^{-2}), with well established fabrication processes. The optomechanical device, shown in the lower inset of Fig. 1A, is designed using finite-element modeling, such that the patterned nanobeam confines light in the telecom band, while at the same time exhibiting a co-localized mechanical breathing mode at $\omega_m = 2\pi \times 2.7$ GHz (Fig. 1B). The electro-mechanical coupling in our device is due to the piezoelectric effect that allows for the excitation of traveling acoustic waves which drive the OMC [22]. The opto-mechanial coupling, on the other hand, is facilitated by the parametric coupling between the mechanical excitation and the intracavity photon number owing to the combination of photoelastic coupling and moving boundary conditions [36]. Both effects can intrinsically operate in a bi-directional and noiseless fashion. The device fabrication consists of a two-stage lithography process to define the IDT and then pattern the nanobeams, followed by an HF etch to remove the AlGaAs sacrificial layer. A final deposition of 5 nm of AlO_x passivates the surfaces and reduces the effect of unwanted drive-laser absorption [38] (see Supplementary Information for details). The lower inset of Figure 1A displays a scanning electron microscope image of an optomechanical device, and an evanescently coupled waveguide which provides optical-fiber access to the confined optical mode [29].

We perform an initial characterization of the device properties at room temperature with the setup depicted in Figure 1C, the results of which are presented in Figure 1D. An S_{11} measurement of the IDT shows a 10 MHz-wide microwave resonance centered at 2.76 GHz. The mechanical mode of the OMC is then measured by locking a laser onto the blue sideband ($\omega_l = \omega_c + \omega_m$) of the optical cavity resonance ω_c ($\omega_c = 2\pi \times 194.3$ THz, with a loaded optical quality factor $Q_o = 3.3 \times 10^4$, see SI), and monitoring the high-frequency noise in the reflected signal. The peak in the noise spectrum at 2.744 GHz corresponds to the thermally-occupied mechanical mode (~1×10^3 phonons) and has a linewidth of several MHz. The small mismatch between the IDT and mechanical resonances of ~10 MHz is a result of fabrication-based inhomogeneities. As we apply an RF tone to the IDT at the mechanical frequency ω_m, we observe an additional narrow peak on top of the thermal noise, corresponding to the transduced coherent signal from the IDT. The height of this peak is dependent on the RF power and the detuning from the mechanical resonance [22].

The room temperature characterization highlights that the large initial thermal occupation of the mechanical mode is a significant source of noise in this conversion process. Especially at low RF drive powers, the thermal noise dominates over the transduced signal [22]. By placing our device in a dilution refrigerator (base temperature ~20 mK), we can in principle reduce the thermal occupation of the mechanical mode to $n_{th} \approx 10^{-3}$. In practice, the achievable occupation is limited by residual heating through laser absorption and finite thermalization to the cryostat [29]. With the device cooled to Millikelvin temperatures, we measure the actual thermal occupation of the mechanical mode by monitoring cavity-enhanced Stokes (blue sideband) and anti-Stokes (red sideband) scattering rates (Γ_B and Γ_R, respectively), when we drive the cavity with laser pulses detuned by $\pm\omega_m$ [27]. We suppress the reflected pump light through spectral filtering, such that only scattered photons on cavity

resonance are detected by superconducting nanowire single-photon detectors (SNSPD) as shown in Figure 2A. Specifically, the rates we measure are set by $\Gamma_B \propto n_{th} + 1$ and $\Gamma_R \propto n_{th}$ [39]. Figure 2B shows the histogram of the single photon count rates measured for 40 ns long pulses set to the two detunings with a peak-power of 107 nW at the device. For this power, we find an optomechanical cooperativity of $C = 1.7$ (see SI) [40]. We extract a thermal occupation of $n_{th} = 0.90 \pm 0.01$, which verifies the initialization of the mechanical mode close to its quantum groundstate. This value is higher than the theoretical value set by the cryostat temperature, limited by residual heating of the structure during the laser pulse [29]. A sweep of the pulse power reveals that lower occupations can be achieved (e.g. $n_{th} = 0.36 \pm 0.03$, see SI), at the cost of a lower conversion efficiency.

We now proceed to verify the conversion from microwave to optical telecom signals at Millikelvin temperatures. Red-detuned ($\omega_l = \omega_c - \omega_m$) optical pulses, which realize an opto-mechanical state-swap [41], are sent into the OMC to read out the state of the mechanical mode, which is coherently excited by sweeping the frequency of an RF drive tone (1 μW) across the mechanical resonance (see Fig. 2C). The data is fitted with a Lorentzian, from which we extract a mechanical linewidth of $\gamma_m/2\pi = 197$ kHz, an expected improvement in mechanical quality factor of about one order of magnitude compared to the value at room temperature. Furthermore, we observe a blueshift of both the mechanical mode and the IDT resonance by about 35 MHz compared to room temperature due to the temperature dependence of the GaAs elastic constants.

While the optical absorption can be reduced through tuning of the power of the input light as well as by pulsed operation, thus far little is known about the potential heating due to the RF tone which drives the IDT. In order to investigate the amount of heating resulting from the RF drive, we measure the second order correlation function $g^{(2)}(\tau) = \left\langle \hat{b}^\dagger(0)\hat{b}^\dagger(\tau)\hat{b}(0)\hat{b}(\tau)\right\rangle / \left(\left\langle \hat{b}^\dagger(0)\hat{b}(0)\right\rangle \left\langle \hat{b}^\dagger(\tau)\hat{b}(\tau)\right\rangle\right)$ of the mechanical resonator mode [29], by swapping mechanical excitations into optical photons at the cavity resonance frequency. Here $\hat{b}\left(\hat{b}^\dagger\right)$ is the annihilation (creation) operator of the mechanical mode. We expect the coherence of the RF drive to be mapped first onto the mechanical state in our resonator and then onto the light field. Any sign of heating due to the RF drive should result in bunching of the $g^{(2)}(\tau)$ during the mechanical lifetime (~1.5 μs). For this measurement, both the laser (locked onto the red sideband) and the RF source are operated in a continuous wave (CW) mode. The scattered optical photons are detected on a Hanbury Brown and Twiss (HBT)-type setup with two SNSPDs. The time τ here is the relative delay between clicks from the two detectors. We observe a near-flat $g^{(2)}(\tau)$ over the entire range of the RF power sweep (see Fig. 2D), clearly indicating that the coherent part of the mechanical state dominates any thermal contribution across the entire power sweep. As a reference, we also perform a measurement without an RF drive but with high enough optical power for absorption-induced heating to occur. In this case, a clear signature of photon bunching is visible, indicating, as expected, a thermal state of the mechanical resonator.

In order to demonstrate the potential of these devices as transducers of microwave to optical signals at the quantum level, we now operate both the RF driving and optical read-out in a pulsed mode [42]. We send a resonant RF pulse (1 μs long) to the IDT to excite our

oscillator and access the mechanical state through a 40 ns long red-detuned state-swap pulse. This allows us to minimize the effects of heating due to optical absorption. The pulsed experiment enables us to quantify the absolute number of coherent phonons added to our initial state by comparing the scattering rate in the presence of an RF drive ($\Gamma_{R,RF}$) to the scattering rate we obtain from the remaining thermal population (Γ_R) (inset in Fig. 3B). By measuring the photon rate with and without a resonant RF drive, we recover an RF-phonon conversion effciency of 3.57×10^{-10} phonons per RF photon.

Using the same HBT-type setup as above, we detect the second order correlation of the scattered photons, which allows us to compare the coincidences between detection events originating from the same ($\Delta i = 0$) or different ($\Delta i \neq 0$) pulse sequences. A selection of the histograms of these correlations is shown in Figure 3A for various coherent phonon occupations (n_{coh}). The full set of $g^{(2)}(0)$ values for increasing coherent phonon occupation is shown in Figure 3B. We expect the value of $g^{(2)}(0)$ to be determined by the ratio n_{coh}/n_{th} (cf. the SI). We extract this number from the relative count rate we recover with and without the RF pulse, $\Gamma_{R,RF}/\Gamma_R$, displayed in the inset of Figure 3B, making use of $\Gamma_R \propto n$. The dashed curve in Figure 3B displays the expected $g^{(2)}(0)$ values for our RF power sweep based on the theory for a displaced thermal state (cf. the SI), which are in good agreement with our measured values. An increase in RF power results in a larger coherent displacement of the thermal state, which in turn leads to a decreased value for $g^{(2)}(0)$.

While our pulsed experiments clearly demonstrate conversion between a coherent state in the microwave and the telecom domain, they do not imply the retention of the input-state phase. In order to access the coherence of the transduction process, we use a modified version of the setup (for a detailed sketch see SI Fig. S5). We split the red-detuned excitation laser into two branches of a phase-stabilized Mach-Zehnder interferometer (MZI), one of which contains our device and the other an amplitude electro-optic modulator (EOM). We drive both the IDT and the EOM with a single RF source, such that a coherent transduction process results in a fixed phase relationship between the up-converted light in the two inteferometer arms. We then mix the light on a beamsplitter, matching the photon rate in the two arms. Figure 4A displays the count rate at one output port of the MZI when we vary the phase of the interferometer for several coherent phonon occupations. We observe a clear interference pattern with a visibility of 44±3% for powers corresponding to a coherent phonon occupation of $n_{coh} = 1.1$, which increases to 85±7% as the coherent contribution dominates over the small thermal background. Figure 4B displays these experimentally retrieved visibilities for several coherent phonon occupations, the expected modeled behavior assuming only thermal noise ($n_{noise} = n_{th}$, solid line), as well as additional incoherent noise sources ($n_{noise} = n_{th} + n_{other}$, dashed line). These respective trends are given by $n\sqrt{\text{coh}/(n_{coh} + n_{noise})}$ and scaled by the maximally achievable interference visibility in our setup of 90%. Here, n_{other} represents the equivalent noise figure for any other source than the thermal occupation of the resonator, including imperfections in the measurement setup. We estimate the upper bound of these sources to be $n_{other} \sim 2.5$. The main contributions to this remaining part are drifts of the interferometer free spectral range over the duration of the measurement, im-perfect sideband resolution $\left((\kappa/4\omega_m)^2 = 0.27\right)$, as

well as mechanical decoherence [16, 24]. This measurement confirms the phase-preserving nature of the conversion process down to the single phonon level.

The total efficiency of our device is the product of two parts: the loading efficiency of the mechanical mode from the microwave side (3.57×10^{-10}, measured from the attenuator output at at the mixing chamber to the excitation of phonons in the mechanical mode) and the optical readout efficiency of the mechanical mode 1.55×10^{-5}. The latter one can itself be separated into two parts: $\eta_{ro} = p_r \times \eta_{det}$, with $\eta_{det} = 1.41 \times 10^{-3}$ (see SI). The state swap probability $p_r = 1.1\%$ is a function of the power with which the optical readout is performed and can be increased through improvements with respect to optical absorption. Note that the current performance of our device is however already sufficient to read out a nonclassical state of the mechanical mode [29]. The low loading efficiency of the mechanical mode can be attributed to the design and size of the electromechanical transducer. We estimate the efficiency of transferring a SAW wave from the IDT (150 μm wide) into a single, narrow (~1 μm), suspended beam to be less than 2.5×10^{-5}. Additional contributions arise from the difference in the polarizations of the incoming SAW wave and the mechanical mode, the discrepancy between the IDT and mechanical frequencies, as well as the large electrical impedance of the IDT. These factors can be improved by tailoring the size and design of the electromechanical transducer specifically to the purpose of exciting the breathing mode of a single nanobeam [43]. While the small-scale piezo-resonator required to mode-match the nanobeam will necessitate careful electrical impedance matching, the required network falls into the range accessible with coplanar resonator technology [43]. The relatively small optomechanical state-swap probability and detection efficiency reported here, on the other hand, can be circumvented with post-selection techniques routinely used in quantum optics experiments [29, 44].

We have demonstrated faithful conversion of a microwave to an optical signal with only a small added thermal contribution due to the groundstate occupation of the mechanical resonator. Furthermore, these measurements show our ability to detect the displacement amplitude of the initial state in our mechanical resonator down to one phonon, (corresponding to our lowest measured RF power), marking a crucial benchmark for applications in the quantum regime [24]. The device used for this experiment is a fully integrated, on-chip hybrid electro-opto-mechanical system with a mechanical mode as the transducer. We cool this mode to its quantum groundstate using a dilution refrigerator, which allows us to operate directly at the quantum noise limit. This work allows for the on-chip integration of a single-photon RF-source, such as a superconducting qubit [35, 45], which paves the way for building a true quantum network over large distances, based on superconducting nodes. The device we consider here is specifically suited towards heralded entanglement generation between remote superconducting qubits, a protocol which is described in Ref. [24].

While we demonstrate quantum limited noise performance in the readout of the mechanical state, the conversion efficiency is currently limited by low microwave-phonon excitation efficiency. We would like to note that this is not a fundamental limit but rather a result of design choices for this proof-of-principle demonstration. The material itself imposes some limitations on the efficiency, such as the remaining absorption heating and

the relatively low piezoelectric coupling. However, demonstrations of coherent coupling between superconducting qubits and surface acoustic waves in GaAs [35, 45] suggest the latter are highly suitable choices for noise-free carriers of quantum information. Importantly, our system is already operating in the range of optical drive strengths expected for mediating efficient conversion. In particular, the opto-mechanical cooperativity of $C \approx 1.7$ (see SI) is sufficient for efficiently converting GHz phonons into telecom photons.

During the submission process we became aware of related work demonstrating GaAs optomechanical crystal in the low thermal occupation regime [46].

Supplementary Material

Refer to Web version on PubMed Central for supplementary material.

Acknowledgments

We would like to thank Vikas Anant, John Davis, Mark Jenkins, and Clemens Schäfermeier for valuable discussions and support. We also acknowledge assistance from the Kavli Nanolab Delft, in particular from Marc Zuiddam and Charles de Boer. The sample growth was realized in the NanoLab@TU/e cleanroom facility. This project was supported by the Foundation for Fundamental Research on Matter (FOM) Projectruimte grants (15PR3210, 16PR1054), the European Research Council (ERC StG Strong-Q, 676842), and by the Netherlands Organisation for Scientific Research (NWO/OCW), as part of the Frontiers of Nanoscience program, as well as through a Vidi grant (680-47-541/994), the Gravitation program Research Center for Integrated Nanophotonics, and the ARO/LPS CQTS program.

References

[1]. Kelly J, Barends R, Fowler AG, Megrant A, Jeffrey E, White TC, Sank D, Mutus JY, Campbell B, Chen Y, Chen Z, Chiaro B, Dunsworth A, Hoi I-C, Neill C, O'Malley PJJ, Quintana C, Roushan P, Vainsencher A, Wenner J, Cleland AN, and Martinis JM, Nature 519, 66 (2015). [PubMed: 25739628]

[2]. Watson TF, Philips SGJ, Kawakami E, Ward DR, Scarlino P, Veldhorst M, Savage DE, Lagally MG, Friesen M, Coppersmith SN, Eriksson MA, and Vandersypen LMK, Nature 555, 633 (2018). [PubMed: 29443962]

[3]. Hofheinz M, Wang H, Ansmann M, Bialczak RC, Lucero E, Neeley M, O'Connell AD, Sank D, Wenner J, Martinis JM, and Cleland AN, Nature 459, 546 (2009). [PubMed: 19478780]

[4]. Kurpiers P, Magnard P, Walter T, Royer B, Pechal M, Heinsoo J, Salathé Y, Akin A, Storz S, Besse J-C, Gasparinetti S, Blais A, and Wallraff A, Nature 558, 264 (2018). [PubMed: 29899478]

[5]. Liao S-K, Cai W-Q, Liu W-Y, Zhang L, Li Y, Ren J-G, Yin J, Shen Q, Cao Y, Li Z-P, Li F-Z, Chen X-W, Sun L-H, Jia J-J, Wu J-C, Jiang X-J, Wang J-F, Huang Y-M, Wang Q, Zhou Y-L, Deng L, Xi T, Ma L, Hu T, Zhang Q, Chen Y-A, Liu N-L, Wang X-B, Zhu Z-C, Lu C-Y, Shu R, Peng C-Z, Wang J-Y, and Pan J-W, Nature 549, 43 (2017). [PubMed: 28825707]

[6]. Boaron A, Boso G, Rusca D, Vulliez C, Autebert C, Caloz M, Perrenoud M, Gras G, Bussières F, Li M-J,Nolan D, Martin A, and Zbinden H, Phys. Rev. Lett 121, 190502 (2018). [PubMed: 30468607]

[7]. Kimble HJ, Nature 453, 1023 (2008). [PubMed: 18563153]

[8]. Witmer JD, Hill JT, and Safavi-Naeini AH, Opt. Express 24, 5876 (2016). [PubMed: 27136784]

[9]. Fan L, Zou C-L, Cheng R, Guo X, Han X, Gong Z, Wang S, and Tang HX, Sci. Adv 4, eaar4994 (2018). [PubMed: 30128351]

[10]. Wang C, Zhang M, Chen X, Bertrand M, Shams-Ansari A, Chandrasekhar S, Winzer P, and Lončar M, Nature 526, 101 (2018).

[11]. Rueda A, Sedlmeir F, Collodo MC, Vogl U, Stiller B, Schunk G, Strekalov DV, Marquardt C, Fink JM, Painter O, Leuchs G, and Schwefel HGL, Optica 3, 597 (2016).

[12]. O'Brien C, Lauk N, Blum S, Morigi G, and Fleischhauer M, Phys. Rev. Lett 113, 063603 (2014). [PubMed: 25148328]

[13]. Hisatomi R, Osada A, Tabuchi Y, Ishikawa T, Noguchi A, Yamazaki R, Usami K, and Nakamura Y, Phys. Rev. B 93, 174427 (2016).

[14]. Stannigel K, Rabl P, Sørensen AS, Zoller P, and Lukin MD, Phys. Rev. Lett 105, 220501 (2010). [PubMed: 21231374]

[15]. Bochmann J, Vainsencher A, Awschalom DD, and Cleland AN, Nature Phys. 9, 712 (2013).

[16]. Andrews RW, Peterson RW, Purdy TP, Cicak K, Simmonds RW, Regal CA, and Lehnert KW, Nature Phys. 10, 321 (2014).

[17]. Bagci T, Simonsen A, Schmid S, Villanueva LG, Zeuthen E, Appel J, Taylor JM, Sørensen A, Usami K, Schliesser A, and Polzik ES, Nature 507, 81 (2014). [PubMed: 24598636]

[18]. Laer RV, Patel RN, McKenna TP, Witmer JD, and Safavi-Naeini AH, APL Photonics 3, 086102 (2018).

[19]. Moaddel Haghighi I, Malossi N, Natali R, Di Giuseppe G, and Vitali D, Phys. Rev. Applied 9, 034031 (2018).

[20]. Suchoi O, Ella L, Shtempluk O, and Buks E, Phys. Rev. A 90, 033818 (2014).

[21]. Vainsencher A, Satzinger KJ, Peairs GA, and Cleland AN, Appl. Phys. Lett 109, 033107 (2016).

[22]. Balram KC, Davanc MI¸Song o, J. D., and Srinivasan K, Nature Photon. 10, 346 (2016).

[23]. Higginbotham AP, Burns PS, Urmey MD, Peterson RW, Kampel NS, Brubaker BM, Smith G, Lehnert KW, and Regal CA, Nature Phys. 14, 1038 (2018).

[24]. Zeuthen E, Schliesser A, Sørensen AS, and Taylor JM, Phys. Rev. Applied 10, 044036 (2018).

[25]. Chan J, Alegre TPM, Safavi-Naeini AH, Hill JT, Krause A, Gröblacher S, Aspelmeyer M, and Painter O, Nature 478, 89 (2011). [PubMed: 21979049]

[26]. Teufel JD, Donner T, Li D, Harlow JW, Allman MS, Cicak K, Sirois AJ, Whittaker JD, Lehnert KW, and Simmonds RW, Nature 475, 359 (2011). [PubMed: 21734657]

[27]. Meenehan SM, Cohen JD, MacCabe GS, Marsili F, Shaw MD, and Painter O, Phys. Rev. X 5, 041002 (2015).

[28]. O'Connell AD, Hofheinz M, Ansmann M, Bialczak RC, Lenander M, Lucero E, Neeley M, Sank D, Wang H, Weides M, Wenner J, Martinis JM, and Cleland AN, Nature 464, 697 (2010). [PubMed: 20237473]

[29]. Hong S, Riedinger R, Marinković I, Wallucks A, Hofer SG, Norte RA, Aspelmeyer M, and Gröblacher S, Science 358, 203 (2017). [PubMed: 28935767]

[30]. Chu Y, Kharel P, Renninger WH, Burkhart LD, Frunzio L, Rakich PT, and Schoelkopf RJ, Science 358, 199 (2017). [PubMed: 28935771]

[31]. Lee KC, Sprague MR, Sussman BJ, Nunn J, Langford NK, Jin X-M, Champion T, Michelberger P, Reim KF, England D, Jaksch D, and Walmsley I, Science 334, 1253 (2011). [PubMed: 22144620]

[32]. Riedinger R, Wallucks A, Marinković I, Löschnauer C, Aspelmeyer M, Hong S, and Gröblacher S, Nature 556, 473 (2018). [PubMed: 29695844]

[33]. Ockeloen-Korppi CF, Damskägg E, Pirkkalainen J-M, Asjad M, Clerk AA, Massel F, Woolley MJ, and Sillanpää MA, Nature 556, 478 (2018). [PubMed: 29695847]

[34]. Meenehan SM, Cohen JD, Gröblacher S, Hill JT, Safavi-Naeini AH, Aspelmeyer M, and Painter O, Phys. Rev. A 90, 011803 (2014).

[35]. Moores BA, Sletten LR, Viennot JJ, and Lehnert KW, Phys. Rev. Lett 120, 227701 (2018). [PubMed: 29906138]

[36]. Chan J, Safavi-Naeini AH, Hill JT, Meenehan S, and Painter O, App. Phys. Lett 101, 081115 (2012).

[37]. Skauli T, Kuo PS, Vodopyanov KL, Pinguet TJ, Levi O, Eyres LA, Harris JS, and Fejer MM, J. Appl. Phys 94, 6447 (2003).

[38]. Guha B, Marsault F, Cadiz F, Morgenroth L, Ulin V, Berkovitz V, Lemaître A, Gomez C, Amo A, Combrié S, Gérard B, Leo G, and Favero I, Optica 4, 218 (2017).

[39]. Safavi-Naeini AH, Chan J, Hill JT, Alegre TPM, Krause A, and Painter O, Phys. Rev. Lett 108, 033602 (2012). [PubMed: 22400740]

[40]. Hill JT, Safavi-Naeini AH, Chan J, and Painter O, Nature Commun. 3, 1196 (2012), 1206.0704. [PubMed: 23149741]

[41]. Galland C, Sangouard N, Piro N, Gisin N, and Kippenberg TJ, Phys. Rev. Lett 112, 143602 (2014). [PubMed: 24765960]

[42]. Riedinger R, Hong S, Norte RA, Slater JA, Shang J, Krause AG, Anant V, Aspelmeyer M, and Gröblacher S, Nature 530, 313 (2016). [PubMed: 26779950]

[43]. Wu M, Zeuthen E, Balram KC, and Srinivasan K, arXiv:1907.04830 (2019).

[44]. Marinković I, Wallucks A, Riedinger R, Hong S, Aspelmeyer M, and Gröblacher S, Phys. Rev. Lett 121, 220404 (2018). [PubMed: 30547658]

[45]. Gustafsson MV, Aref T, Kockum AF, Ekström MK, Johansson G, and Delsing P, Science 346, 207 (2014). [PubMed: 25213379]

[46]. Ramp H, Hauer B, Balram K, Clark T, Srinivasan K, and Davis J, arXiv:1812.09417 (2018).

[47]. Oz-Vogt J, Mann A, and Revzen M, J. Mod. Opt 38, 2339 (1991).

[48]. Marian P and Marian TA, Phys. Rev. A 47, 4474 (1993). [PubMed: 9909456]

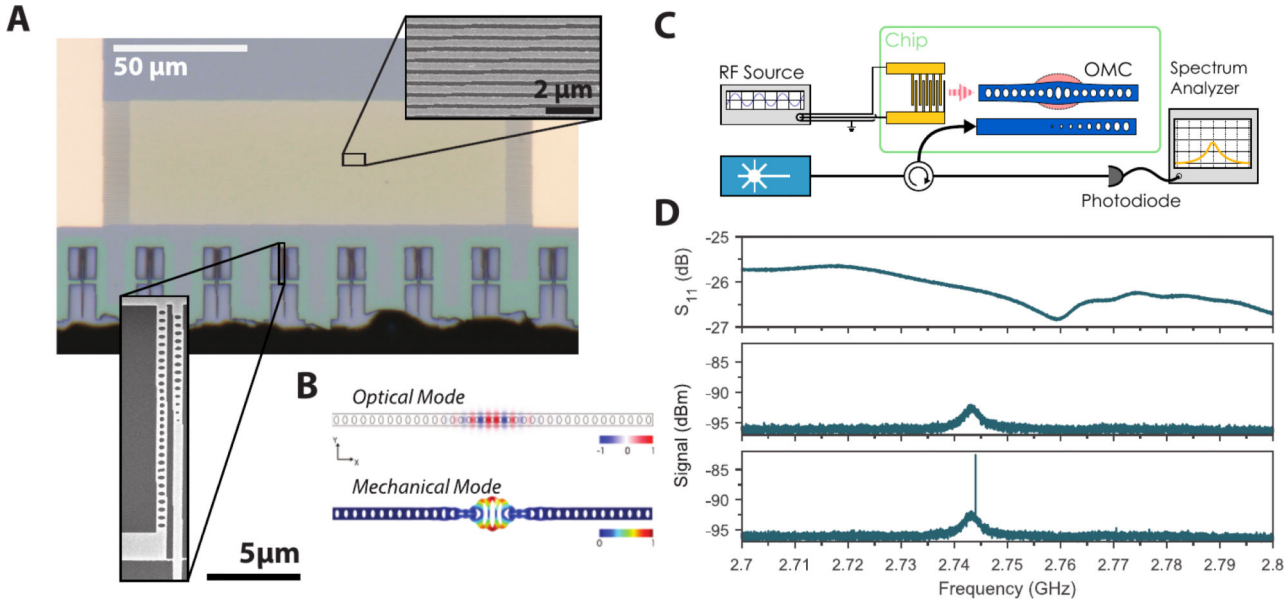

FIG. 1. Device layout and room temperature characterization.

(A) Microscope image of the transducer devices: Our structures are comprised of an interdigital transducer (IDT, in gold, cf. upper inset), which spans several optomechanical devices for ease of fabrication. The bottom side of the chip is directly accessible with a lensed fiber, allowing for optical access to the devices. The lower inset contains a scanning electron microscope image of an optomechanical resonator. The waveguide (right) is used for evanescently coupling light in and out of the device using the lensed fiber (accessed from the bottom, not shown). (B) Finite element simulations of the optomechanical device. The E_y component of the fundamental optical mode is shown (top) alongside the displacement field of the co-localized mechanical mode oscillating around 2.7 GHz (bottom). (C) Schematic of the room temperature characterization setup. A laser is used to address the device optically. The reflected light is then measured on a high-speed photodiode to resolve the noise spectrum around the mechanical frequency while an RF source is used to drive the IDT. (D) (Upper Panel) S_{11} reflection measurement of the IDT device with a resonance at 2.76 GHz. (Lower Panels) Optical measurements of the GHz-frequency noise of the reflected light with (bottom) and without (center) the RF drive tone applied to the IDT, which results in a narrow, coherent peak in the spectrum on top of the thermal peak. The laser in these measurements is blue-detuned from cavity resonance by the mechanical frequency, ω_m.

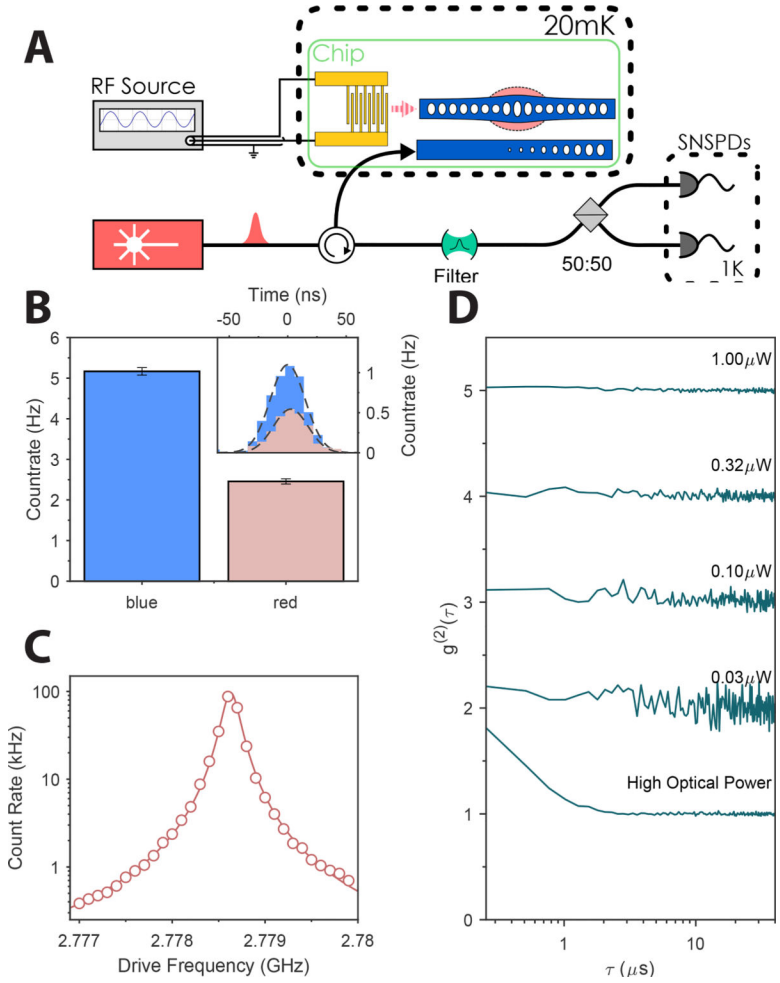

FIG. 2. Device characterization at Millikelvin temperatures.

(A) Schematic of the cryogenic experimental setup. The sample with the OMC and IDT, as well as a pair of superconducting nanowire single photon detectors (SNSPDs) are placed inside the dilution refrigerator (at 20 mK and ~1 K, respectively). We lock the laser on the red sideband of our cavity and filter residual reflected pump light from the cavity, detecting photons scattered on the cavity resonance. (B) Sideband thermometry to extract the thermal occupation of the mechanical resonator. We find an occupancy $n_{\mathrm{th}} = 0.9 \pm 0.01$, confirming the initialization of the device close to its quantum groundstate. The bar graph shows the integrated counts for the red and blue sideband drives as well as the corresponding histograms (inset). Errors are one standard deviation, owing to the shot noise resulting from photon counting. (C) Mechanical characterization and initial RF to telecom-band conversion at mK temperatures. We sweep the RF drive frequency with the laser locked at $\omega_c - \omega_m$ and monitor the count rate. The solid curve is a Lorentzian fit to the data, from which we extract a mechanical linewidth of 197 kHz, corresponding to a mechanical lifetime of ~0.8 μs. (D) Hanbury Brown and Twiss-type measurement of the photons emitted from our cavity with 7 nW of optical input power. The second order correlations $g^{(2)}(\tau)$ are shown for a selection of the measured RF powers alongside a reference measurement with no RF drive, but high optical power (4.5 μW, bottom curve). The curves are offset for clarity. The bunching in

the reference measurement results from absorption heating due to the laser drive, yielding a large thermal state of the mechanical resonator.

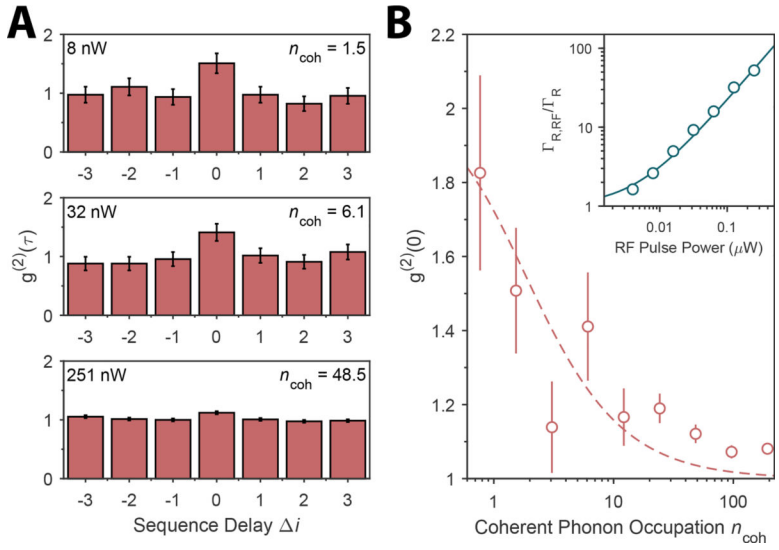

FIG. 3. Correlation measurements of the microwave-to-optical transducer in the pulsed regime.
(A) The transducer is operated such that RF drive pulses are upconverted to the optical domain using optical readout pulses. Shown are the correlations between coinciding detection events on the two single-photon detectors for photons emerging from the same $\Delta i = 0$ or different $\Delta i \neq 0$ pulse sequences. The panels correspond to various coherent phonon populations. (B) The full set of $g^{(2)}(0)$ values is shown as a function of RF power applied to the IDT. The dashed curve displays the expected value of $g^{(2)}(0)$ for a displaced thermal state with the corresponding extracted coherent phonon number n_{coh} (see SI). The inset shows the relative increase in the count rate as a function of RF power with a linear fit. We use this to extract the ratio of n_{coh}/n_{th}, which allows us to demonstrate the conversion at the single coherent phonon level for the lowest powers. We can see a clear transition from a bunched (low RF power) towards a not-bunched (high RF power) second order correlation.

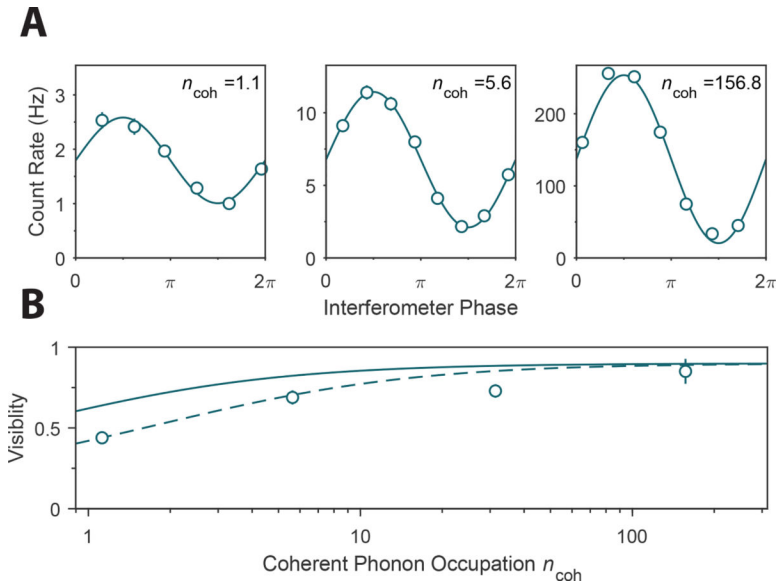

FIG. 4. Preservation of phase coherence during transduction.

(A) Interference patterns taken at different values of n_{coh}. The solid curves are sinusoidal fits to the data, from which we extract the visibility. (B) Visibility as a function of the coherent phonon occupation in the mechanical resonator. The error in the visibility for the lower values of n_{coh} are smaller than the data point size. The data is overlaid with the expected visibility from the coherent and noise contributions $\sqrt{n_{coh}/(n_{coh}+n_{noise})}$. The solid line considers thermal noise only ($n_{noise} = n_{th}$), while the dashed line also takes any other sources into account ($n_{noise} = n_{th} + n_{other}$), while both are scaled by the maximum available visibility in our setup.